Modeling

P. Spädtke, GSI Darmstadt

1 Introduction

Modeling is the task to define a correct picture of a physical device described by rules which can be handled by a computer. Because here we are at the CAS for ion sources we restrict ourself to ion sources, ion beams and related topics. Charged particles are influenced by electric and magnetic fields, and they produce such fields by their own. To solve the equation of motion all participating fields have to be known: the electric field $\vec{\mathbf{E}}$ and the magnetic flux density $\vec{\mathbf{B}}$. These fields might be either static or time dependent, in general they are not symmetric but are real 3D fields. Depending on the number of charged particles, fields will be created by their own: $\vec{\mathbf{E}} = \vec{\mathbf{E}}_{\mathbf{ext}} + \vec{\mathbf{E}}_{\mathbf{int}}$, and $\vec{\mathbf{H}} = \vec{\mathbf{H}}_{\mathbf{ext}} + \vec{\mathbf{H}}_{\mathbf{int}}$.

In times when computer did not exist, analytic models were required to estimate unknown field distributions or an experimental method like the electrolytic trough had to be used. Today differential equations can be solved with numerical methods and therefore it is possible to predict the behavior of physical systems by digital computers. However, the applied models have to describe correctly the real behavior. Let us assume a specific case to demonstrate the problem: a drifting ion beam. No external fields are present and no time dependency is assumed in this case.

2 Drifting Ion Beam

If all external fields are known, the solution of the initial value problem needs to be solved. The easiest case is when all external fields disappear: $\vec{\mathbf{E}} = \mathbf{0}$ and $\vec{\mathbf{H}} = \mathbf{0}$. Let us assume a beam tube of 80 mm diameter and 1 m length, see Figure 1. Discretization is made by a grid of 100 nodes in each cartesian direction. This gives a longitudinal resolution of 1 cm, and a transverse resolution of 1 mm.

Because no external electric fields (grounded beam tube) and no internal magnetic fields (electric current is negligible) are present, the final coordinates x_f, y_f, z_f of each particle are easy to calculate, and are given by:

$$x_f = x_0 + v_x \cdot t \tag{1}$$
$$y_f = y_0 + v_y \cdot t \tag{2}$$
$$z_f = z_0 + v_z \cdot t \tag{3}$$

If the initial conditions $(x_0, y_0, z_0, v_x, v_y, v_z)$ are known, the final coordinates can be calculated exactly, and the problem has been solved.

However, it is well known, that charged particles will repel each other if they are of the same sign. These fields are generated by all participating particles, described by their space charge:

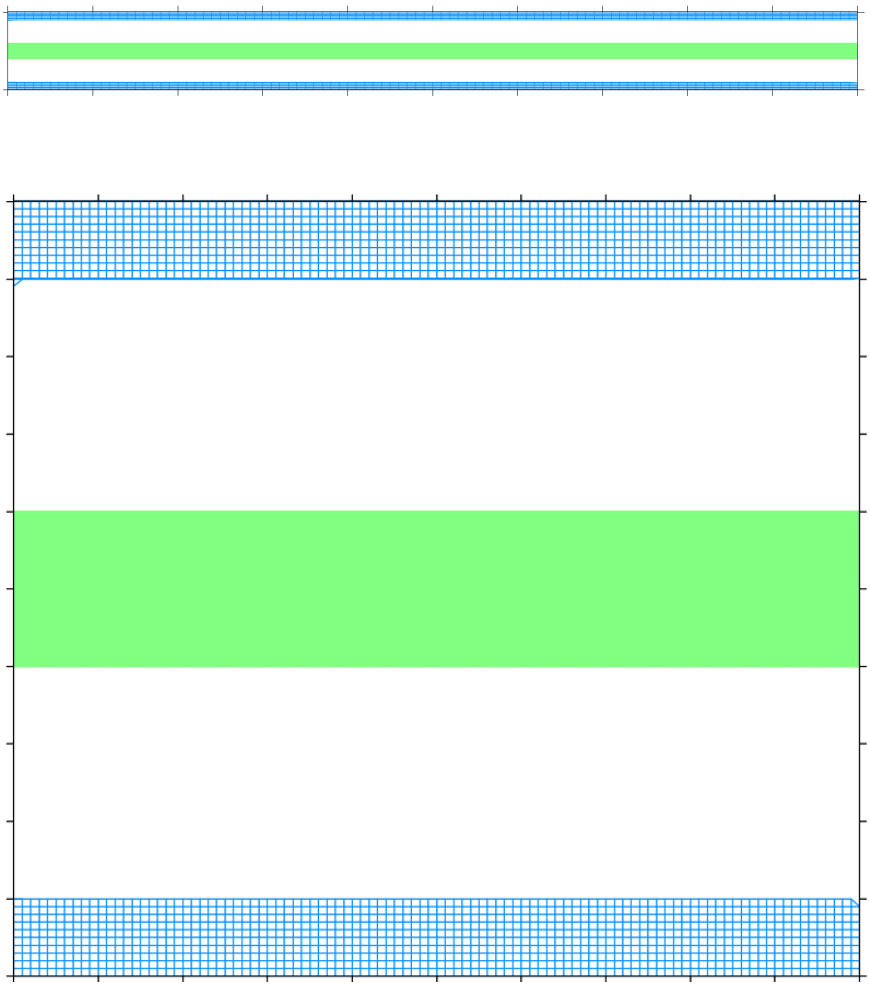

Figure 1: Drifting ion beam in a beam tube of 1 m length and 80 mm diameter. The beam tube is indicated by the blue mesh. The ion beam drift energy of singly charged Argon ions is assumed with 35 keV. The trajectories are shown in green. Top: Correct geometric scaling, bottom: scaling differently in horizontal and vertical direction, to show more details. Beam radius is 10 mm.

$$\rho = \vec{I}/(\varepsilon_{\mathbf{0}} \cdot \vec{\mathbf{v}}) \tag{4}$$

where I is the current in A, v the velocity of the charged particle in m/s, ε_0 the permittivity in vacuum, and ρ the resulting space charge. The space charge of such a beam is shown in Figure 2.

This space charge produces an electric potential Φ as shown in Figure 3, described by Poisson's equation, for which the Cartesian formulation is shown in Equ. 5. The resulting electric fields will influence the particles themselves.

$$\partial^2\Phi/\partial x^2 + \partial^2\Phi/\partial y^2 + \partial^2\Phi/\partial z^2 + \rho/\varepsilon_0 = 0 \tag{5}$$

Only a few problems can be solved analytically, for example an infinitely long ion beam, homogeneously distributed space charge, drifting with a constant velocity.

If this is not the case, the differential equation (Equation 5) is to be replaced by a difference equation for each node point. Boundary conditions have to be defined at all six surfaces of the surrounding box. Each difference equation can than be solved consecutively. With a successive over relaxation method the set of equations can than be solved much faster. The result of such a simulation is shown in Figure 3. Differences in computing time are demonstrated in Figure 12.

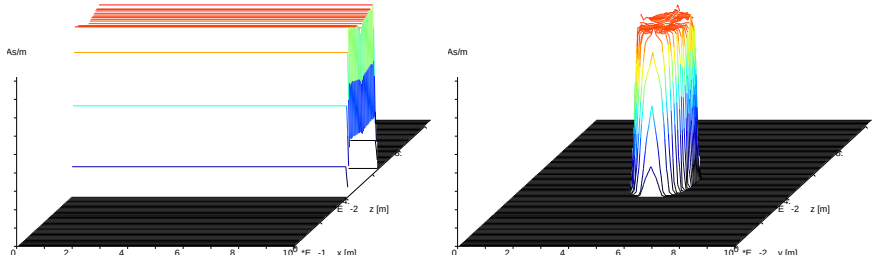

Figure 2: Charge density distribution of the drifting ion beam. Left: in beam direction, right: perpendicular to beam direction.

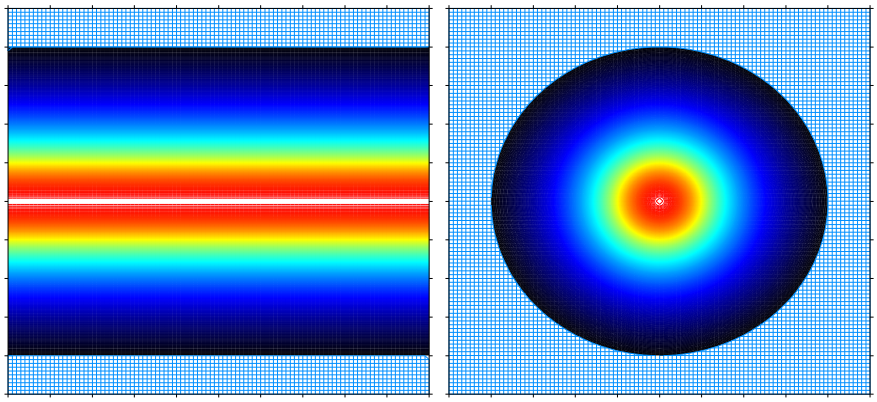

Figure 3: Electric potential caused by the charge density, as shown in Fig. 2, I = 5 mA.

This simulated potential distribution can be compared with the analytic expression: for a infinitely long, cylindrical ion beam with zero emittance, carrying the current I with constant drift velocity the potential Φ can be calculated analytically as function of the radius r:

$$\Phi(r) = \frac{I}{4\pi\epsilon_0 v} \cdot \left(1 + 2 \cdot \ln\frac{r_b}{r} - \frac{r^2}{r_b^2}\right); \textbf{if} \quad r \leq r_b \tag{6}$$

with the velocity v, permittivity ϵ_0, and beam pipe radius r_b. Outside the beam the potential is:

$$\Phi(r) = \frac{I}{2\pi\epsilon_0 v} \cdot \left(\frac{1}{2} + \ln\frac{r_b}{r}\right); \textbf{if} \quad r \geq r_b \tag{7}$$

For a singly charged Argon ion beam of 5 mA and an energy of 35 keV the program predicts 412 V on axis for the given ratio of beam tube diameter to beam diameter.

The magnetic field of the drifting ion beam (an azimuthal component $B_\Theta(r)$ of about $1{\cdot}10^{-6}$ T at the beam edge) can be neglected at velocities in the order of $\beta \approx 0.1\%$:

$$B_\Theta(r) = -\frac{\mu_0 \cdot I}{2 \cdot \pi \cdot r} \tag{8}$$

With Equations 6 and 7 the correct space charge treatment by the program can be checked, but of course, this solution is not a self consistent solution. The interaction of the electric field with the particles is neglected. The self consistent solution can be obtained by a successive repetition of solving Poisson's equation and the equation of motion, which creates the space charge map. This procedure converges in most cases to the self consistent solution.

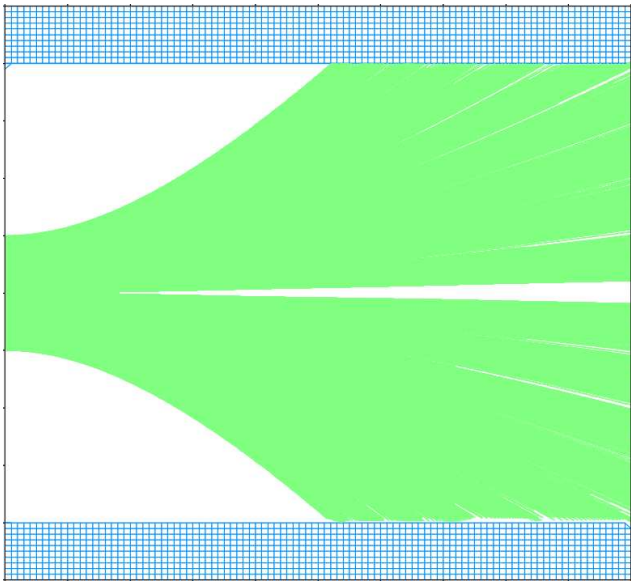

Figure 4: Self consistent solution of the drifting ion beam of 5 mA without any space charge compensation.

Beside the repulsive force of particles with the same sign of charge, the force is contractive for charges of different sign. A positive ion beam tries to attract electrons, and if the space charge of ions cancels the space charge of electrons no repulsing force is acting at all. This process is called space charge compensation. The effect can be measured and has been measured [1], but how to model? The simplest method is to assume a net current.

2.1 Linear Compensation

Instead of taking the full current into consideration (5 mA) only the uncompensated fraction is used for the simulation. Assuming a space charge compensation of 90%, the current used for the simulation is only 0.5 mA. This assumption however excludes non linear interaction of both particle groups. The resulting trajectory plot is shown in Figure 5, different projections of the 6D phase space into 2D sub spaces are shown in Figure 6

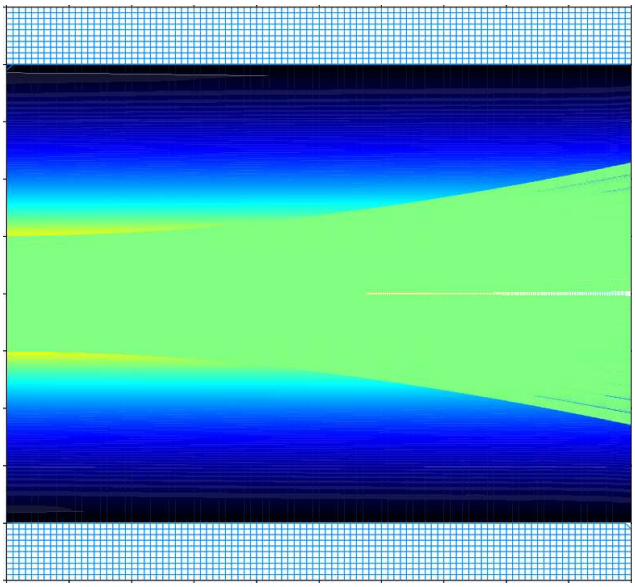

Figure 5: Self consistent solution of the drifting, partially compensated ion beam, plotted together with the potential distribution, assuming a linear space charge compensation. Active current 0.5 mA, respectively 90% space charge compensation.

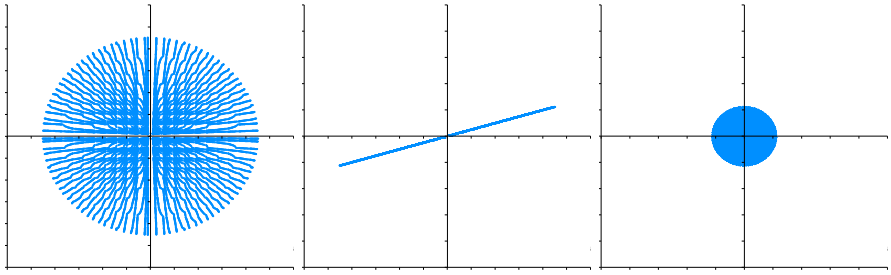

Figure 6: Beam profile, emittance, and momentum space at the end of the drift section, assuming 90% linear space charge compensation.

2.2 Ion Beam Plasma, Analytic Solution

A better approach is to assume, that the remaining uncompensated charges leads to a beam plasma potential. This assumption creates a field free region within the beam, but with an electric gradient at the beam boundaries. The trajectory plot is shown in Figure 7, the resulting potential distribution is shown in Figure 8, whereas different projections of the 6D phase space to 2D sub spaces are shown in Figure 9. Instead of defining the degree of space charge compensation, the value of the resulting space charge potential has to be given. In our case, a beam plasma potential of 50 V would roughly correspond to 90% space charge compensation.

2.3 Creation of Secondaries

A third approach is to model the generation of secondaries. In that case the neutral gas pressure in the beam line has to be known, as well as the cross sections for the different assumed processes: Ion-ion collisions might take place, as well es electron-

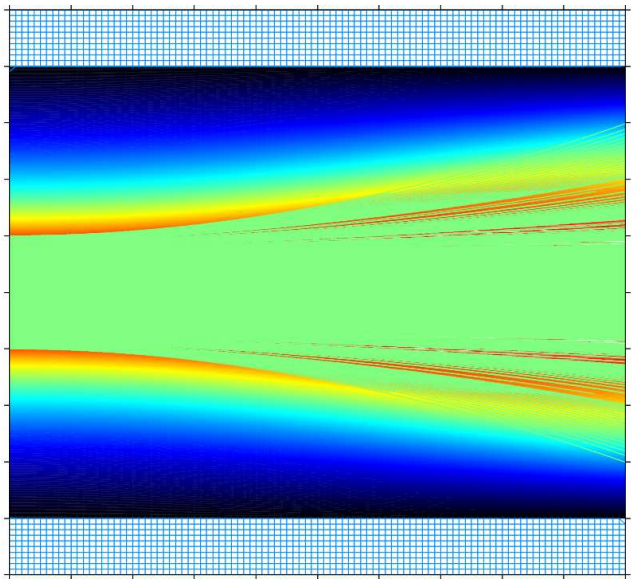

Figure 7: Self consistent solution of the drifting ion beam, plotted together with the potential distribution, assuming a beam plasma of 50 V.

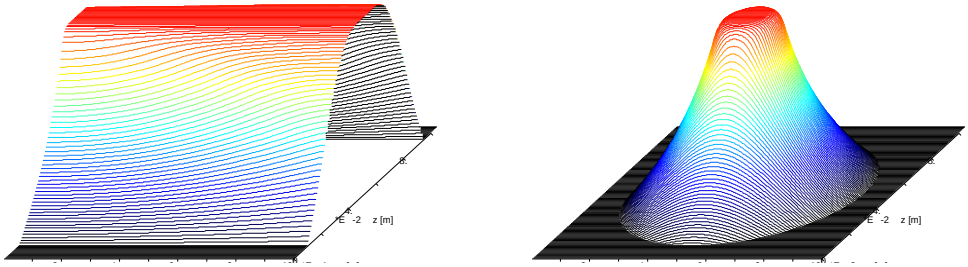

Figure 8: Self consistent potential distribution generated by the drifting ion beam in beam direction (left), and perpendicular to the beam direction (right).

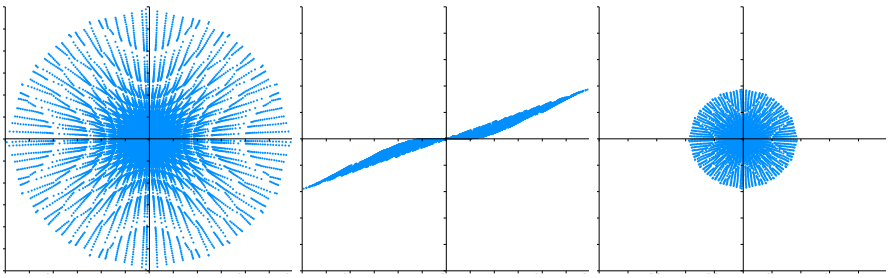

Figure 9: Beam profile, emittance, and momentum space at the end of the drift section for the beam plasma compensation model.

ion collisions, ion-neutral collisions, only to mention a few of possible interactions. In Figure 10 a realistic neutral gas density distribution is shown. Together with correct cross section and the primary ion intensity the rate of secondaries can be calculated. The resulting secondaries can be used to distribute their space charge

in addition to the space charge of primary ions.

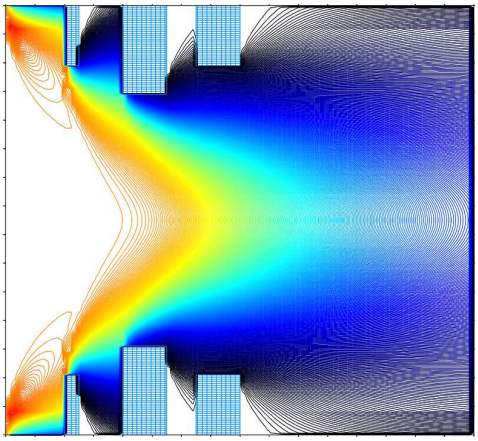

Figure 10: Neutral gas pressure caused by the ion source which can be used for the generation of secondaries.

Because the number of secondaries for each primary trajectory should be large to minimize the discretization error, the total number of trajectories could become too high for a reasonable solution time.

When the development with time is to be simulated, another dimension has to be added, and a PIC code is required. An example is given in [2].

Up to now, we have assumed, that the beam is infinitely long, and its generation is located in infinitely distance. In most cases this is not true, and any modeling needs to assume something like a source for the simulated ion beam. Therefore the question arises how to model. This will be covered in the section 4.

3 Solver

Some general remarks should be made about the method of solving. Different numerical methods are available to solve a huge set of equations. Each method might have advantages and disadvantages. For the kind of modeling we are talking about a point-to-point solver has the big advantage that analytic expressions can be used on each point for example to calculate the electron density term as defined in Equation 10 or the secondary ion density term in Equation 12. In case of a direct solver, the iterative determination of electron density would not be possible and the correct simulation of a plasma boundary would fail.

The rate of convergence depends on several aspects: the total number of nodes to be calculated, see Figure 11, the question whether different mesh distances are used or not, whether an over relaxation method is applied, see Figure 12.

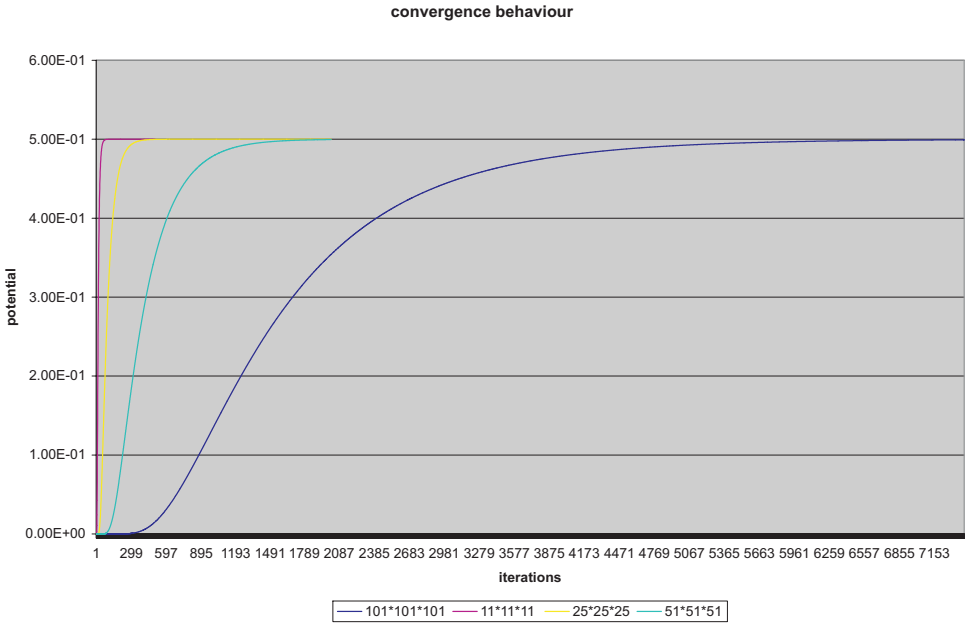

Figure 11: Convergence behavior: number of nodes. The more nodes are to be calculated, the more iterations are required to achieve sufficient precision [3].

The necessary CPU time to run such a bench mark is given in Table 1: Laplace solver on a 2D-grid with 101 times 101 nodes and defined boundary condition.

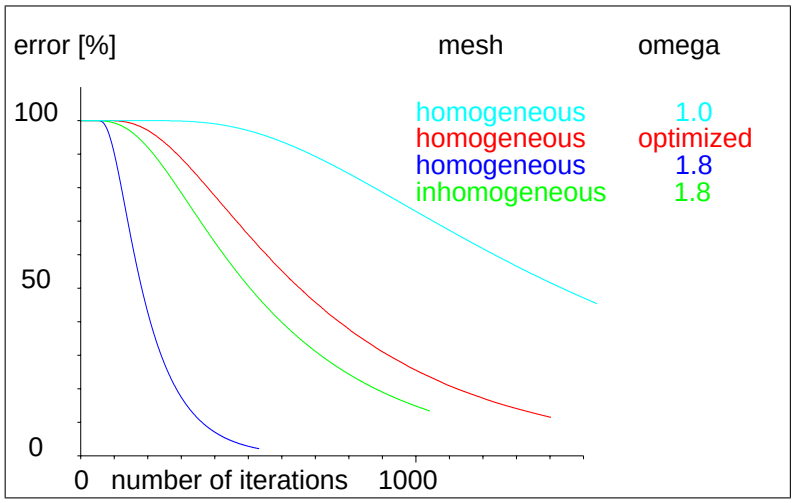

Figure 12: Convergence behavior: Deviation of the analytical correct value in the center of a simulation as function of the iteration count. The influence of a mesh with variable mesh distances or constant mesh distances and the influence of the over relaxation parameter is shown.

Computer	Language	single precision	double precision
McIntosh	Pascal*	60000	—
McIntosh	Basic*	54000	—
Commodore C64	Assembler	18000	—
Atari ST	GFA Basic*	7720	—
Atari ST	Assembler	1800	—
HP9816	Basic*	7710	—
IBM PC	Fortran	7055	—
IBM XT/8087	Fortran	1723	—
VAX 8700	Fortran	10.5	15.8
IBM 3090-200	Fortran	2.61	—
Cray XM-P	Fortran	2.2	—
today's laptop	Fortran	0.031	0.031

Table 1: Necessary CPU time for different hardware. The asterisk indicates that an interpreter instead of a compiler has been used. The data beside the today's laptop data have been compiled already in 1987 [4]

4 Particle Sources

Even that the general method to extract a charged particle from a particle source seems to be similar (biasing the particle source positively, to extract positive charges from the source) mostly any particle source requires its own model.

4.1 Fixed cathode

The first model which was implemented in computer codes was the model of cathode emission of electrons from a solid cathode surface. This model is also applicable to surface ionization sources.

$$j = \frac{4\varepsilon_0}{9}\sqrt{\frac{2q}{m}}\frac{\Phi^{3/2}}{d^2} \tag{9}$$

The Child-Langmuir law (Equation 9) describes the particle density or here the electron current as function of the applied extraction voltage.

A successive iteration scheme (solving Poisson's equation, followed by solving Lorentz equation) will modify Φ and therefore the current density. The modeling requires a slow increase of the current density, not to run into convergence problems.

It should be mentioned, that this assumption is valid only, if the emission is space charge limited, and not emission limited. In the second case, the achievable current density is of course below the current density described in Equation 9. With this restriction, the model can also be applied for the simulation of surface ionization sources.

4.2 Plasma Sources - no Magnetic Field

4.2.1 Volume Ion Sources

Volume ion sources have a radial magnetic confinement, but the magnitude of $\vec{\mathbf{B}}$ is negligible for extracted ions close to the axis. Without extraction voltage the plasma would penetrate into the extraction system, but with positive biasing of the ion source, ions are retracted from the ion source, whereas electrons are reflected back into the source plasma. This can be modeled using Self's[5] theory, describing the electron density n_e as function from the potential Φ:

$$n_e = n_{e0}e^{-\frac{q(\Phi_{pl}-\Phi)}{kT_e}} \tag{10}$$

where n_{e0} the electron density within the undisturbed plasma with plasma potential Φ_{pl}, k is Boltzmann's constant and T_e is the electron temperature. Using Equation 10 an electron term can be added to the space charge ρ in Equation 5. The influence of space charge and space charge compensation can be seen in Fig. 13, where the current density is increased from zero to 1000 A/m^2 (16.8 A/m^2, 75 A/m^2, 100 A/m^2, 500 A/m^2, 750 A/m^2, 1000 A/m^2). For discretization 100 nodes are used in longitudinal direction and 80 nodes in each transverse direction. The resolution is than in the range of 200 μm. The potential at the three electrodes is 20 kV, -20 kV, and 0 kV.

The plasma boundary develops as shown in Figure 14. The plasma boundary is visualized by plotting a few potential lines close to the plasma potential.

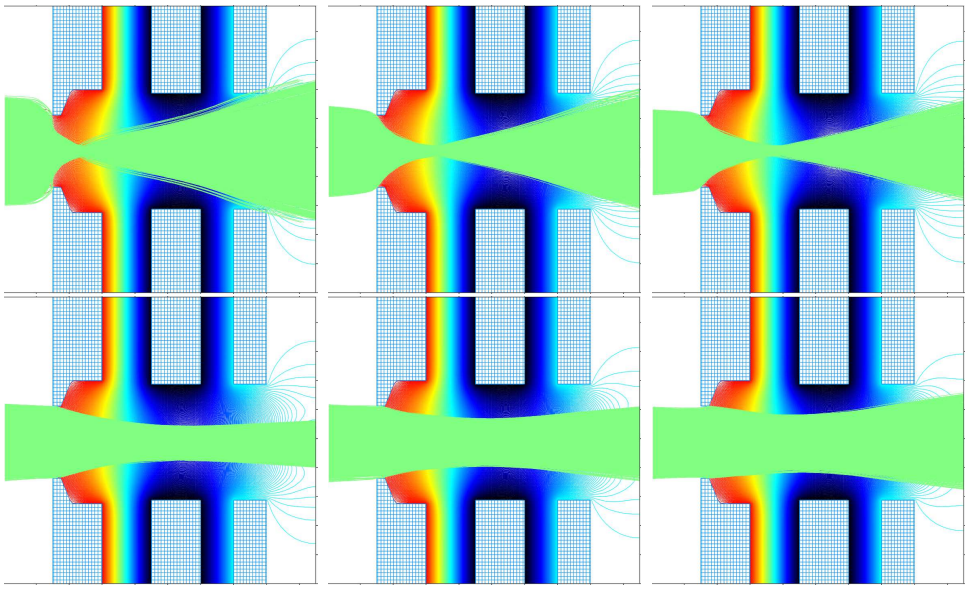

Figure 13: Beam profile with increasing particle density.

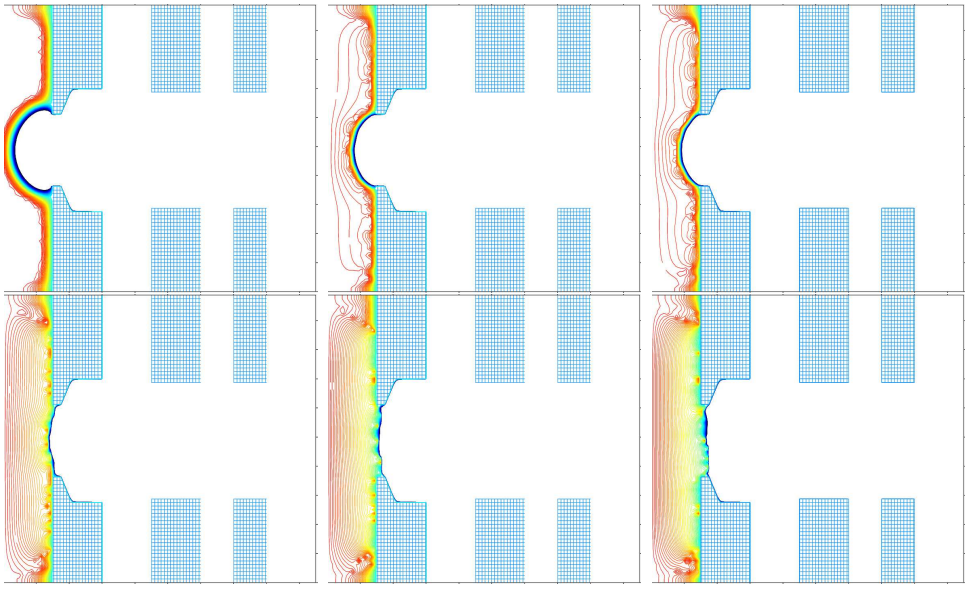

Figure 14: Plasma boundary with increasing particle density.

4.2.2 Laser Ion Sources

Laser ion sources creates a plasma by focusing a powerful laser beam onto a solid target. The temperature of the target close to the focal point increases drastically until the target material evaporates and becomes ionized. The starting velocity perpendicular to the target surface is not negligible.

Furthermore, the time of laser irradiation is very short, in the order of ps. If a drift section inside the plasma chamber (before extraction) is used to increase the pulse length, the extraction voltage has to be ramped to avoid a different energy along the pulse. A large momentum spread is typical for laser ion sources. Longitudinal effects become important, and a Particle In Cell (PIC) code might become

necessary. As long as these effects can be neglected, a trajectory code can be used when the additional starting velocity is taken into account.

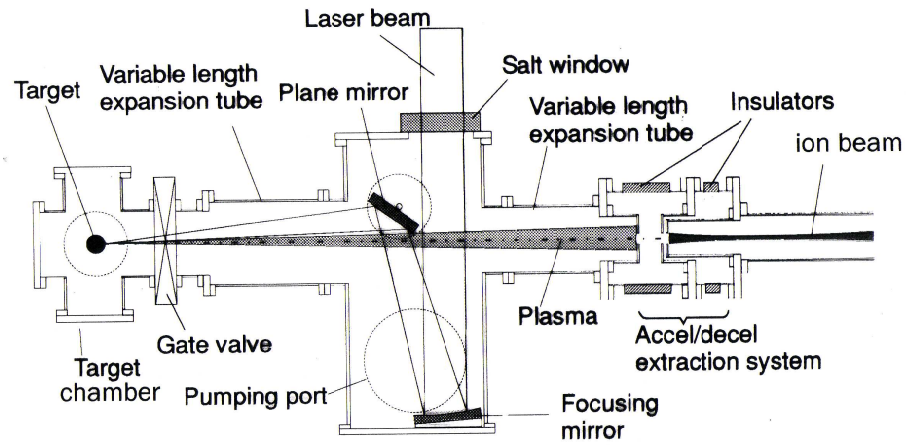

Figure 15: CO_2-laser ion source[6]. The long drift space from the laser target to the extraction system allows the particles to de-bunch. As a result, the high current density decreases, but the pulse length increases.

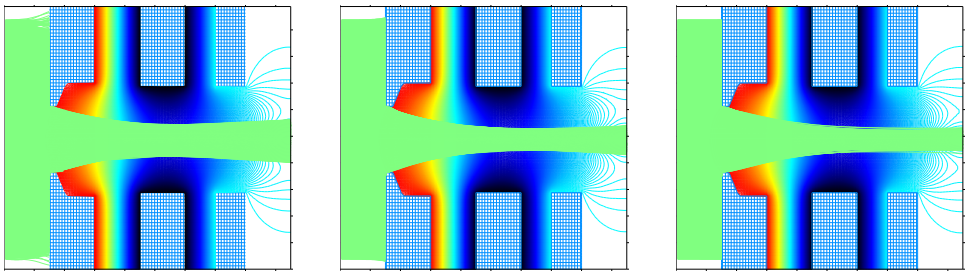

Figure 16: With increasing laser power the ions have larger velocity.

In case of a much more powerful laser, not only higher particle densities can be achieved, but also the first section of the linear accelerator can be replaced. High energies, up to the MeV-range have been measured for protons created by laser radiation[7]. For such a simulation not only protons with a large momentum distribution are taken into account, but also co-moving electrons which compensate the space charge of the ions.

4.3 Plasma Sources - with Magnetic Field

4.3.1 PIG Ion Sources

There are different technical solutions available for a PIG ion source. One main classification might be the direction of extraction, which is either in radial or in axial direction (with respect to the anode). Here only the radial extraction system is covered[8]. If the source is operated in sputter mode, an additional electrode is introduced into the plasma chamber, electrically insulated against the annular anode tube. Typically this sputter electrode made from the desired material, is biased negatively with respect to the anode. A certain fraction of ions which are present from the main gaseous discharge inside the anode chamber will be accelerated towards the sputter electrode. Depending on the material, sputter voltage and mass of primary ions neutral atoms can reach the discharge chamber, where they eventually becomes ionized.

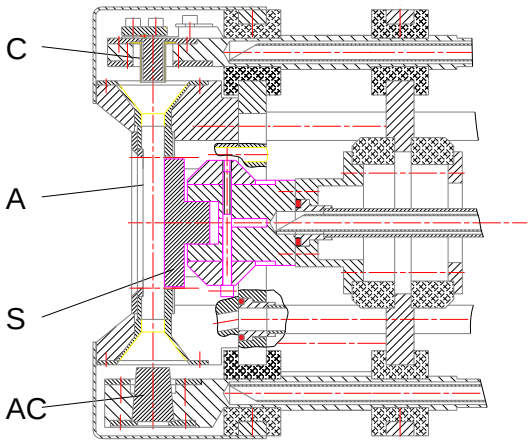

Figure 17: Radial extraction from a Penning ion source. C cathode, AC anti-cathode, S sputter electrode, A anode. Simulations have been made for gaseous operation, see Figures 18, 19, 20 and for the sputter mode, see Figures 21, 22. The magnetic field direction is within the plane of plotting in direction from the cathode to anti-cathode.

To increase the efficiency of the discharge, the complete ion source is embedded in a strong magnetic field (several kG). The electron density can be increased by this method. Simultaneously the extracted ions are affected by this magnetic field, shown in Figure 23. The path length of the ions within the magnetic field is in the range of several 10 cm. Space charge compensating electrons would not be able to move freely in that region. Nevertheless, experimentally experience show that the extracted ion beam has to be space charge compensated. Otherwise the obtained electrical currents would not be possible. Obviously, electrons are present within the magnetic field, where they can move (oscillate) along the magnetic field lines.

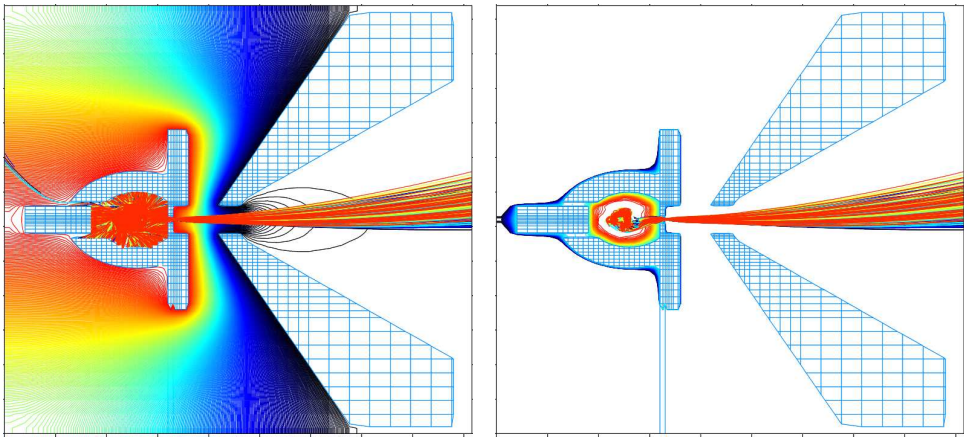

Figure 18: Radial extraction from a Penning ion source (no sputtering). Left: all trajectories plotted, right: only ion trajectories which are extracted are shown. Low current mode ($\approx$ total 50μA).

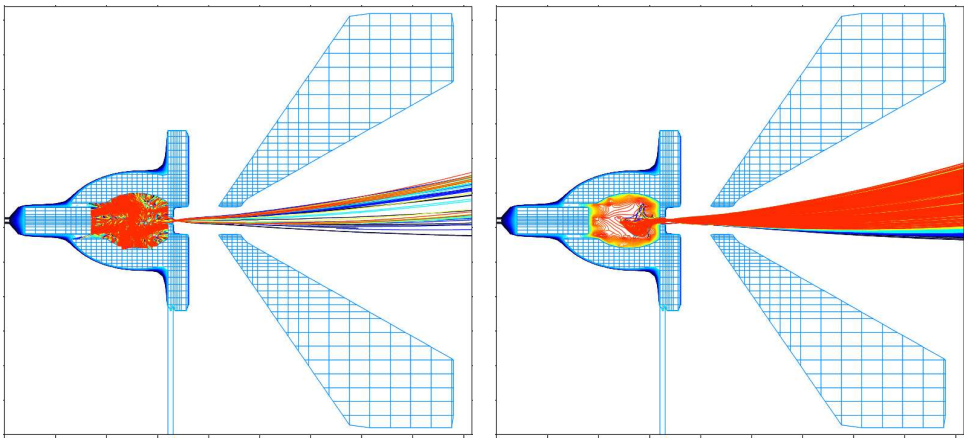

Figure 19: Radial extraction from a Penning ion source (no sputterering), higher current density ($\approx$ total 1 mA). Left: all trajectories plotted, right: only ion trajectories which are extracted are shown.

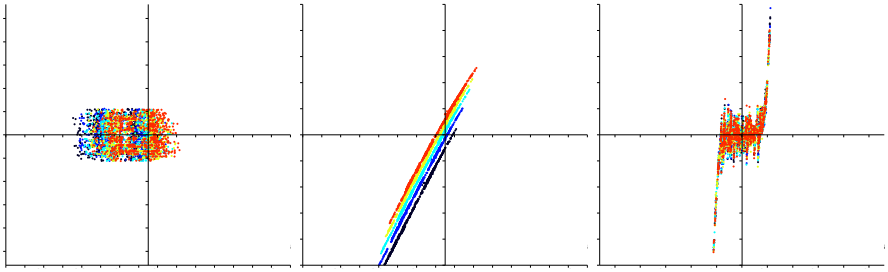

Figure 20: Radial extraction from a Penning ion source (no sputtering). Left: real space, middle: horizontal emittance (perpendicular to the slit direction), right: vertical emittance (slit direction). Higher current mode ($\approx$ total 1 mA).

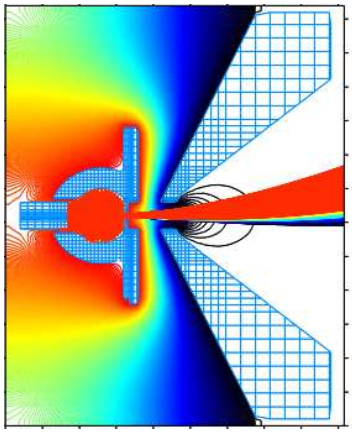

Figure 21: Radial extraction from a Penning ion source in sputter mode.

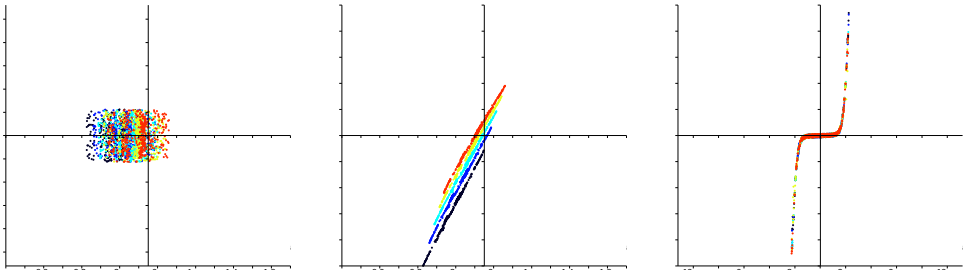

Figure 22: Radial extraction from a Penning ion source in sputter mode. Low current mode ($\approx$ total 50μA).

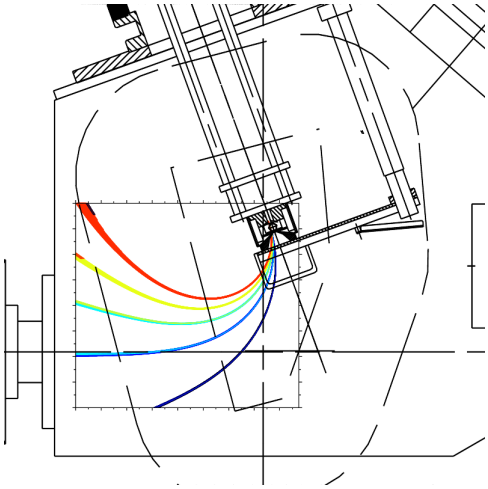

Figure 23: Top view of a PIG source with an extraction system inside a 110^0 source dipole magnet, and the vacuum beam line. The rectangular insertion shows the region of computation together with an extracted Argon beam with charge states 1 to 5. Charge state 2 has been selected for the accelerator. A fully space charge compensated beam is assumed. As starting coordinates for the ions the output coordinates from the extraction simulation have been used.

4.3.2 ECR Ion Sources

Electron Resonance Cyclotron Ion Sources (ECRIS) have a strong axial magnetic mirror field. A radial multipole component (in most cases a hexapole) is added to increase the radial confinement and to stabilize the plasma confinement, especially for higher particle densities. Electrons are magnetized under the influence of the strong magnetic flux densities in the order of a few Tesla. Because of the low temperature of ions, they are magnetized as well. The property 'magnetized' means that the Larmor radius described in Equation 11 is small compared to other dimensions.

$$r_L = \frac{mv_\perp}{qB} \tag{11}$$

Some examples, with the assumption of a certain voltage drop (here 5 Volt) and a given magnetic flux density (here 1 Tesla) are given in the following table:

	mass	charge	velocity	$r_L(1T)$
electron	e	-1	1 327 075 ms^{-1}	$7.50 \cdot 10^{-6}$ m
ion	p	1	30 971 ms^{-1}	$0.32 \cdot 10^{-3}$ m
ion	Ar	10	9 793 ms^{-1}	$0.41 \cdot 10^{-3}$ m
ion	Xe	10	8 525 ms^{-1}	$1.17 \cdot 10^{-3}$ m
ion	U	1	2 000 ms^{-1}	$4.97 \cdot 10^{-3}$ m
ion	U	28	10 620 ms^{-1}	$0.94 \cdot 10^{-3}$ m

Because of the magnetization the trajectories of ions inside the plasma are not affected, or at least not strong affected, by ion-ion collisions. Ions as well as electrons can move freely along a magnetic field line, and depending on the gradient of the magnetic flux density along the magnetic field line, energy in direction of the magnetic field line is transferred into the plane perpendicular to the magnetic field line and vice versa. Ions can be extracted from the ion source, even if they are generated at any place within the plasma chamber far away from the extraction aperture. Especially in the configuration of an ECRIS this is equivalent to the fact, that ions are generated at different levels of magnetic flux density[9]. This means for this specific ion source, that not only $\int \vec{B} ds \neq 0$, but furthermore $\int \vec{B} ds$ is different for ions coming from different starting points. These different initial condition has to be taken into account when modeling ECRISs.

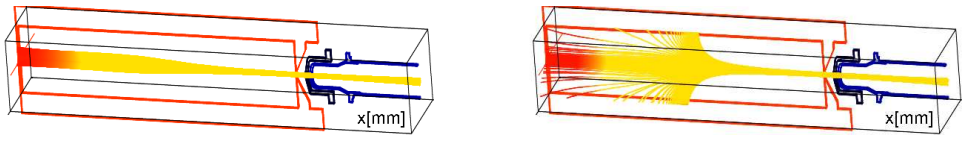

Figure 24: Magnetic field lines going through the extraction aperture on a circle of 5 mm for two different magnetic settings.

Of course, the magnetic field distribution is not a free parameter to optimize the condition for a good extraction. It has to be chosen according physical boundary conditions and to provide a good plasma confinement.

The magnetic field lines can now be used to localize the starting locations of the ions, see Figure 24. Depending on the specific magnetic setting, ions from different locations are extracted. The color along the field line indicates the relative

magnetic flux density compared to the flux density at the extraction aperture. In this example, the magnetic flux density is such as high, that the ion beam will be focused after extraction already in the fringing field of the solenoid. The following profiles and emittance figures are taken at different locations of the beam line: 0.75 m 0.8 m, 0.85 m and 0.9 m, see Figure 25. The different colors for different particles in Figure 26 indicate different initial magnetic flux density at the origin of particles.

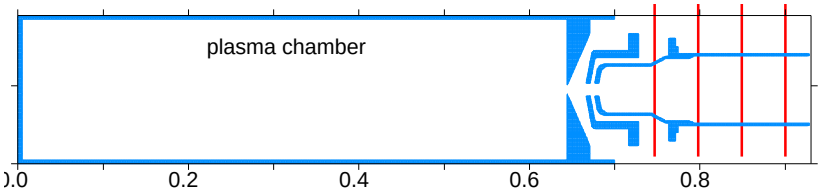

Figure 25: Horizontal projection of the extraction system of the MS-ECRIS including plasma chamber. The red lines indicate the four locations of the given profiles, respectively emittances.

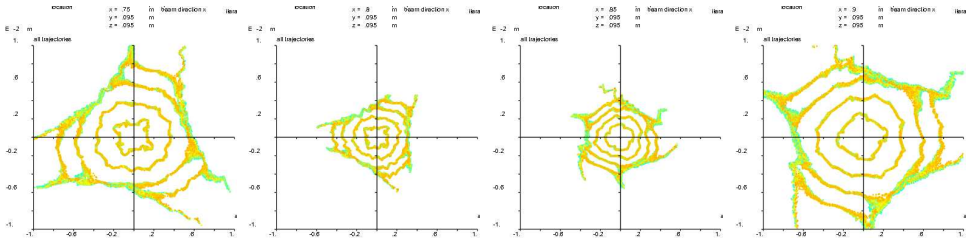

Figure 26: Real space (profile) at 0.75 m, 0.8 m 0.85 m, and 0.9 m. Scale is ±1 cm.

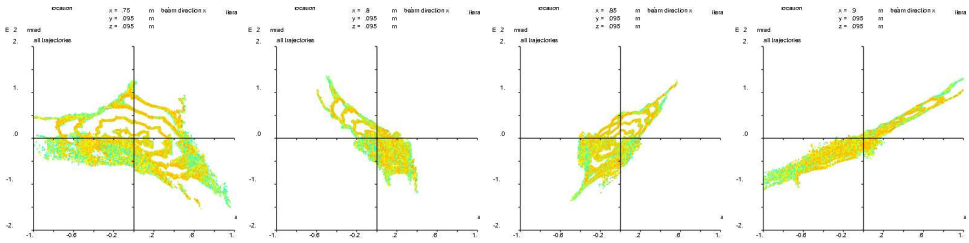

Figure 27: Horizontal emittance at the same position. Scale is ±1 cm, respectively ±200 mrad.

These kind of structures as can be seen in the profiles of Figure 26, have been observed experimentally. This confirm that the assumptions are realistic, but the model is of course not complete. The distribution needs to be smoothed, here only magnetic field lines going through the extraction hole on 1 mm, 2 mm, 3 mm, and 4 mm radius have been used. A charge state distribution has to be used instead of only one charge state. Furthermore the particle density at different places inside the plasma chamber has to be known. Experiments with variable frequency have shown a strong influence on the extracted beam intensity [10].

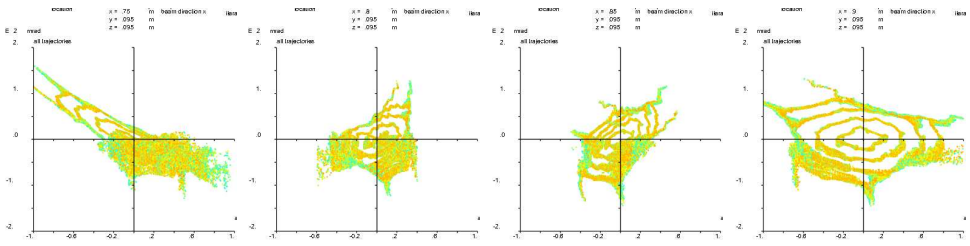

Figure 28: Vertical angles as function from horizontal location (mixed phase space). Scale is ±1 cm, respectively ±200 mrad.

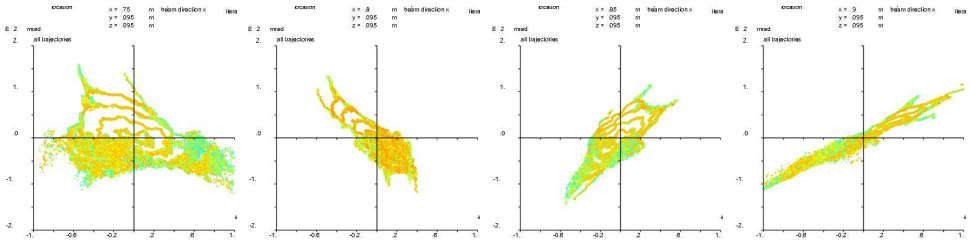

Figure 29: Vertical emittance. Scale is ±1 cm, respectively ±200 mrad.

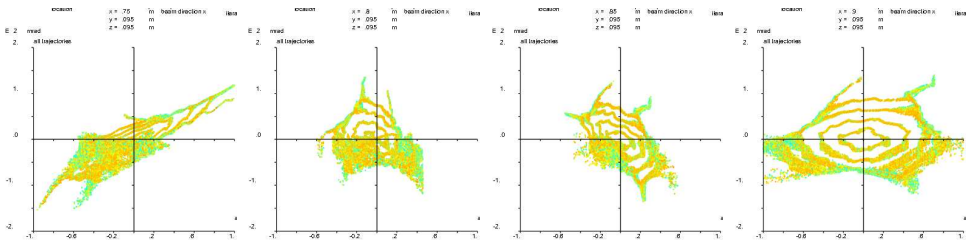

Figure 30: Horizontal angles as function from vertical location (mixed phase space). Scale is ±1 cm, respectively ±200 mrad.

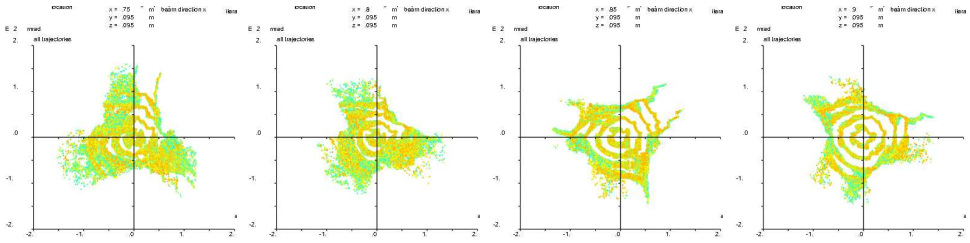

Figure 31: Momentum space ±200 mrad in both directions.

For this simulation 450 nodes in longitudinal direction, and 201 nodes in each transverse direction have been used, in total 28 350 450 nodes. For one charge state about 100 000 trajectories are necessary. Computing time including space charge, a full spectrum is in the order of several hours.

4.3.3 Negative Ion Sources

For negative ion beam extraction the neutralization of electrons and negative ions inside the plasma is performed by positive ions.

$$n_{i+} = n_{i0} e^{-\frac{q(\Phi - \Phi_{pl})}{kT_i}} \tag{12}$$

where n_{i+} is the density of positive ions as function from the potential Φ. The number of positive ions within the undisturbed plasma is n_{i0} at plasma potential Φ_{pl} with an ion temperature of T_i. This equation is similar to the case of the positive ion sources (Equation refplasma boundary pos), but positive ions play the role of electrons within the plasma. For extraction of H^- the source has to be biased negatively, but this will extract electrons as well. Because the electron density can be high compared to negative ions, the load of the undesired electrons for the power supply is high. Typically, a magnetic filter is used at a position close to the extraction electrode to prevent electrons from extraction. The magnetic field can be produced by permanent magnets, or by a coil inside the plasma chamber. The coil is indicated by the black conductor, shown in Fig. 32 and 34. However, the magnetic field influences not only the electrons, but also the extracted negative ions. The extracted negative ions do have an angle which might have to be compensated.

In the first example, the location of the magnetic filter is too close to the extraction system. A lot of electrons will be extracted, see Figure 32 and 33.

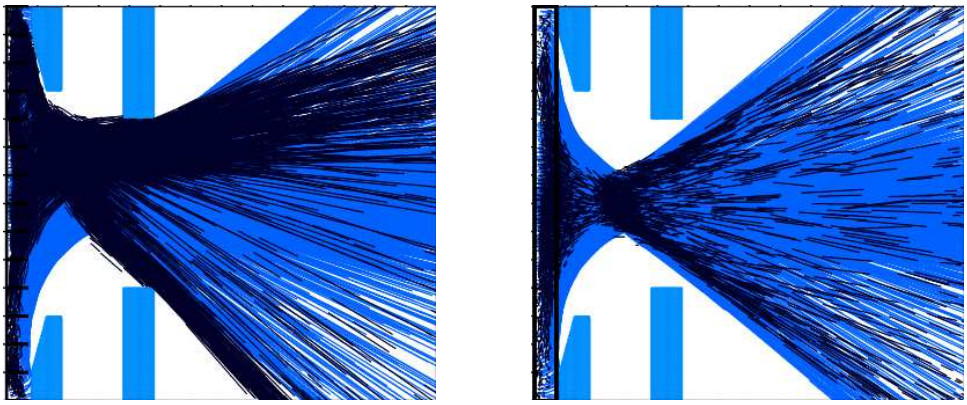

Figure 32: Horizontal and vertical projection of extraction geometry together with the ion and electron trajectories. The magnetic flux density in this case is not strong enough to retain the electrons from being extracted.

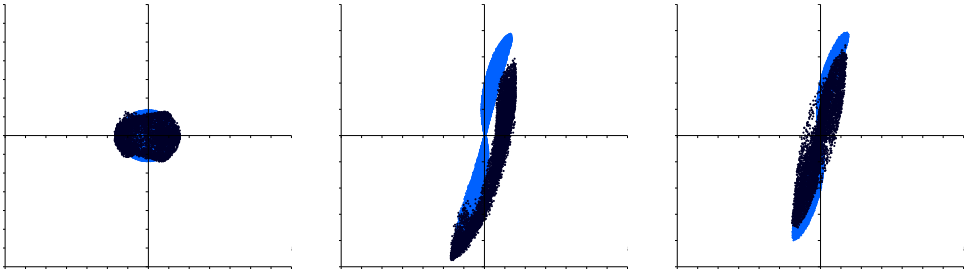

Figure 33: Real space, Horizontal and vertical emittances. H^- in blue, electrons in black.

To improve the action of the filter it has been moved 4 mm back in plasma direction. In Figure 34 it is shown, that this modification was successful; all electrons remain within the plasma.

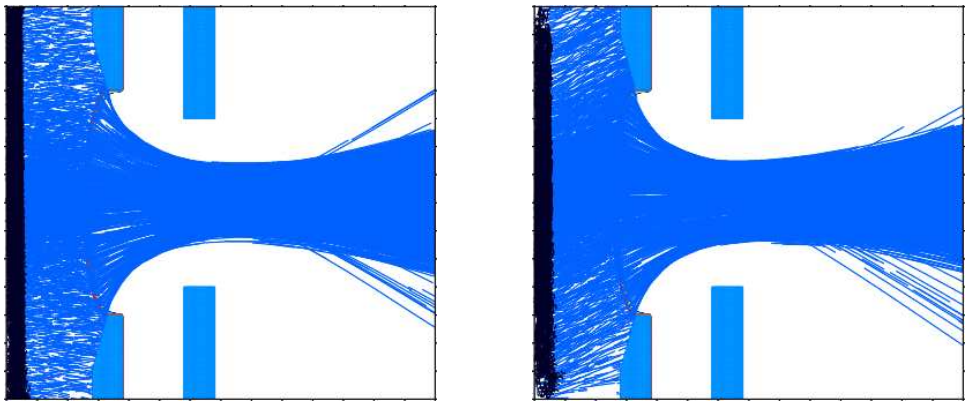

Figure 34: Plasma boundary and extracted H^--beam in blue. Electrons are trapped within the plasma.

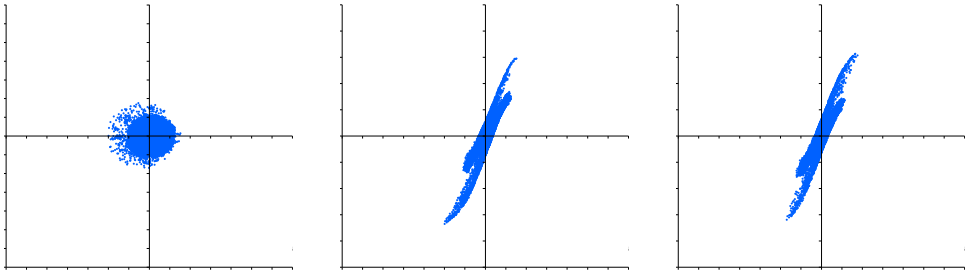

Figure 35: Real space, horizontal and vertical emittances. H^- in blue, electrons are trapped within the plasma.

It should be noted, that all other parameters beside the relative position of the magnetic filter are unchanged. In both cases a H^- current density of 2000 Am^{-2} and an electron current density of 8000 Am^{-2} has been assumed.

For this simulation 401 nodes in longitudinal direction, and 201 nodes in each transverse direction have been used, in total 16 200 801 nodes. For the simulation of H^- 50 000 trajectories and 10. 000 trajectories for electrons have been used. Computing time including space charge is in the order of several hours.

References

[1] R. Dölling, J. Pozimski, P. Groß, J. Klabunde, and P. Spädtke; Investigation of Space-Charge Compensation with Residual-Gas-Ion Energy analyser. Proceedings of the XVIII International Linear Accelerator Conference; ISBN 92-9083-093-X (1996).

[2] N. Chauvin, O. Delferrière, R. Duperrier, R. Gobin, P.A.P. Nghiem, and D. Uriot, Transport of intense ion beams and space charge compensation issues in low energy beam lines. Proceedings of the 14^{th} International Conference on Ion Sources, Review of Scientific Instruments, Vol. 83, Number 2, 2012.

[3] From the KOBRA3-INP user manual, INP, Junkernstr. 99, 65205 Wiesbaden, Germany.

[4] The Physics and Technology of Ion Sources, edited by I.G. Brown; John Wiley & Sons, ISBN 0-471-85708-4 (1989)

[5] S.A. Self, Phys. Fluids 6, p. 1762, 1963.

[6] V. Dubenkov, B. Sharkov, A. Golubev, A. Shumshurov, O. Shamaev, I. Rudskoy, A. Streltsov, Y. Satov, K. Makarov, Y. Smakovsky, D. Hoffmann, W. Laux, R.W. Müller, P. Spädtke, C. Stöckl, B. Wolf and J. Jacoby, Acceleration of Ta^{10+} ions produced by laser ion source in RFQ MAXILAC. Laser and Particle Beams, 14, pp 385-392. 1996.

[7] K. Harres, I. Alber, A. Tauschwitz, V. Bagnoud, H. Daido, M. Günther, F. Nürnberg, A. Otten, M. Schollmeier, J. Schüttrumpf, M. Tampo, and M. Roth; Beam collimation and transport of quasineutral laser-accelerated protons by a solenoidal field, Physics of Plasmas 17, 2010.

[8] P. Spädtke and C. Mühle, Simulation of ion extraction and beam transport, Review of Scientific Instruments, Vol.71, Issue 2, 2000.

[9] P. Spädtke, R. Lang, J. Mäder, F. Maimone, J. Roßbach, K. Tinschert, Investigations on the Structure of the Extracted Ion Beam from an ECRIS, Review of Scientific Instruments, Vol. 83, Issue 2, 2012.

[10] F. Maimone, K. Tinschert, L. Celona, R. Lang, J. Mäder, J. Roßbach, and P. Spädtke; Operation of the CAPRICE electron cyclotron resonance ion source applying frequency tuning and double frequency heating, Review of Scientific Instruments, Vol. 83, Issue 2, 2012.